buildings

MDPI

Article

Influence of Superstructure Pouring Concrete Volume Deviation on Bridge Performance: A Case Study

Jintian Yu, Jinquan Zhang, Pengfei Li and Xu Han *

Research Institute of Highway Ministry of Transport, Beijing 100088, China
* Correspondence: cexuhan@163.com; Tel.: +86-155-2802-2987

Abstract: Due to factors such as casting, mold making, and construction errors, the actual size of the bridge structure will inevitably deviate from the designed size and dimension, and the amount of deviation between the two volumes is generally random and the location of the deviation is not fixed. However, this phenomenon that occurs in the actual practice has not been paid enough attention within existing studies. From a theoretical point of view, the apparent size of concrete will directly affect the cross-sectional stiffness, especially for statically indeterminate structures. This effect will be further reflected in the internal force and stress distribution of the structure. In addition, the variation of the poured volume of the bridge superstructure can also influence the dead-load effect of the bridge structure. Therefore, the influence of pouring concrete volume deviation (PCVD) on the cross-sectional stiffness of large-span continuous reinforced concrete rigid-frame (CRCR) bridges was first stressed and investigated in this paper. Field data of PCVD were monitored by measuring demolished sections with tools that ensure accuracy, and a sensitivity analysis was conducted to analyze the effect of PCVD on the cross-sectional stiffness at different locations. Statistical analysis of the measured data concluded that PCVD has a significant influence on the internal-force distribution and structural stiffness of the bridge, up to 30%. Finally, a theoretical method that considers the influence of PCVD was proposed based on the field monitoring data and the statistical analysis results.

Keywords: volume deviation; cross-sectional stiffness; cantilever casting; continuous rigid-frame bridge

Citation: Yu, J.; Zhang, J.; Li, P.; Han, X. Influence of Superstructure Pouring Concrete Volume Deviation on Bridge Performance: A Case Study. *Buildings* **2023**, *13*, 887. https://doi.org/10.3390/buildings13040887

Academic Editor: Giuseppe Quaranta

Received: 23 February 2023
Revised: 26 March 2023
Accepted: 27 March 2023
Published: 28 March 2023

1. Introduction

In recent decades, continuous rigid-frame bridges have been widely used in the world's infrastructure construction, especially in China. Figure 1 shows the trend and number of continuous reinforced concrete rigid-frame (CRCR) bridges constructed in China [1]. CRCR bridges have been built in large numbers, benefiting from many advantages: (i) more rigidity of the structure; (ii) fewer moments in the deck being partly transferred to the supporting members; and (iii) no bridge bearings are required to be set since the pier and the beam are integrated as one solid structure. At the moment, a large number of studies have been conducted on the mechanical properties and behavior prediction of continuous rigid-frame bridges. The influence factors, such as shear lag [2,3], shear deformation [4–6], temperature stress [7,8], shrinkage, and creep [9], are gradually considered in the mechanical analysis of CRCR bridge, and the cracking and the long-time deflection are of great concern [10,11]. The manual calculation based on formulas is mainly used for theoretical deduction and simple inspection [12,13], and its application in complex structure design and verification is limited. The finite-element method has become an important tool for structural analysis. It has been a research hotspot to reflect the actual performance of the bridge and predict its future behavior by considering the influence of different action factors and updating the finite-element model with measured data [14–19]. This paper shows that the influence of volume deviation caused by construction methods on bridges is not negligible.

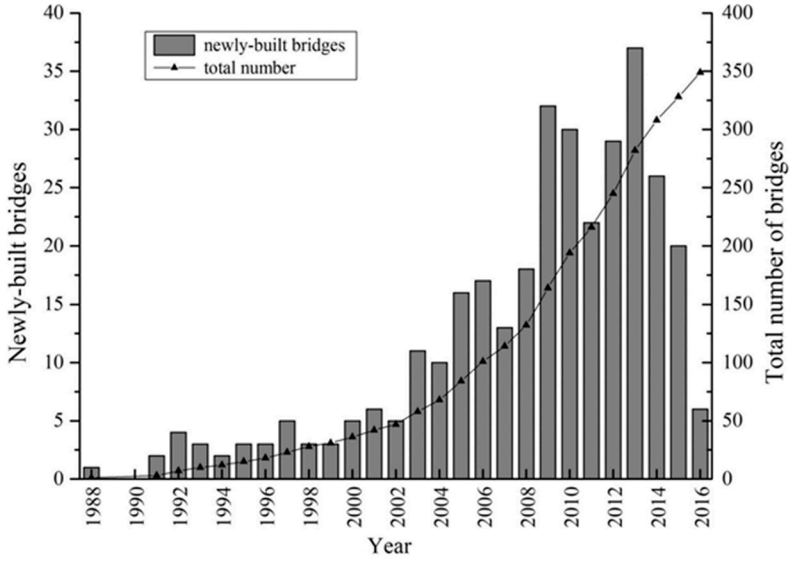

Figure 1. Newly built and total number of continuous reinforced concrete rigid-frame (CRCR) bridges in China [1].

Due to the factors, such as casting mold making and construction operation errors, the bridge structure, inevitably, has the issue of pouring concrete volume deviation (PCVD), which is random in the amount and position. The distribution characteristics of PCVD are unclear, which brings uncertainty to the internal-force calculation and service performance analysis of large-span CRCR bridges. At present, only a few existing studies pay attention to the volume deviation of components. Mutashar R. et al. [20] analyzed the reasons for the deterioration of concrete at the lower edge of hinge joints of hollow-plate small-box girders and believed that the sudden change of contact stress caused by dimensional variation was one of the important reasons. Holicky et al. [21] described the influence of volume deviation on the structure from the design point of view but did not explain its causes. Luo et al. [22] investigated the PCVD of prefabricated concrete components and found that the deviation of prefabricated components was very small, while the PCVD of the cantilever-casting method was unknown. Theoretically, the influence of PCVD on the superstructure of CRCR bridge is mainly reflected in two aspects: one is that the pouring volume is different from the design resulting in uneven dead-load distribution, and the other is that the volume deviation of different parts of the structure results in the inconsistency of structural stiffness. Existing studies cannot explain the effect of PCVD on the service performance of CRCR bridges from the above perspectives.

Currently, hardly any measured data of PCVD about CRCR bridges are available. The detection of PCVD mainly adopts the coring sampling measurement method and non-contact measurement method [23,24]. The coring sampling method is somewhat destructive to the structure. Drilling coring will weaken the section and cause stress redistribution. Moreover, the method can only be used for typical section checks, which is difficult to reflect the overall condition of the bridge due to the limited feasible sampling locations of the bridge. Non-contact measurement mostly adopts a three-dimensional laser point cloud, which is limited by the occlusion of the test perspective, the correction of position coordinates, as well as the test-environment conditions. In practice, it has the shortcomings of low-test efficiency and difficulty to distinguish the main structure from the auxiliary facilities and has not been widely used in the field of bridge dimension identification. In the current AASHTO [25] specification, for structural design, the dead-load coefficient is 1.25, and the Chinese specification [26] considers the dead-load coefficient to be 1.2 when it is unfavorable to the structure. The abovementioned specifications only consider the coefficient that increases the dead load in the calculation and have not yet considered the

influence of volume deviation at different parts on the stiffness of the structure, which results in a conservative design.

In this paper, a finite element model was established to compare and analyze the structural response under dead load and live load, and the influence of PCVD at different positions on the performance of CRCR bridge. Combined with the superstructure demolition and replacement project of four CRCR bridges with main span length of more than 70 m, the concrete pouring condition of different sections of different parts of the continuous rigid-frame bridge was obtained by measuring section by section, and the distribution characteristics of the PCVD of the continuous rigid-frame bridge was analyzed. The influence of volume deviation on the stiffness of the bridge was analyzed, and the correction coefficient considering the change of dead load and stiffness was proposed, which is helpful for the refined design of future bridges and the internal-force calculation of bridges in service.

2. Analysis of Influence of PCVD on Performance of CRCR Bridge

2.1. General

The concrete casting and pouring deviation of the superstructure of a continuous rigid-frame bridge will lead to the variation in dead load and stiffness. The degree of dead-load variation is affected by the pouring deviation value. While the degree of stiffness variation is not only related to the pouring deviation value but also significantly related to the location of the deviation. It is well-known that the farther the cross-section fiber is from the centroid, the greater the contribution of the fiber to the cross-section moment of inertia. A finite element model of an equal-section box girder was established to verify the effect of stiffness variation and internal-force distribution caused by the same ratio of pouring volume deviation in different parts of the top slab, web, and bottom slab. The finite element analysis software ABAQUS is adopted within this paper

2.2. Model Method

2.2.1. Geometric Form

Most long-span continuous rigid-frame bridges adopt beams that vary in height along the length of the bridge span, and the design value of the height–span ratio is generally between 1/12 and 1/25. In this model, the height–span ratio is 1/25 [1], which is also the cross-section form of the main span of bridge B in the Section 3 case study. As shown in Figure 2, in order to facilitate the analysis of the influence of sectional PCVD on the overall performance, the cross-section form is properly simplified and the slabs with haunched ribs and cross slope are eliminated. The main span model with an equivalent equal section is established as shown in Figure 3, with a span of 100 m. This model only considers the contribution of the longitudinal prestressed steel strand to the stiffness of the structure, which is accurate enough to analyze the influence of the pouring volume deviation.

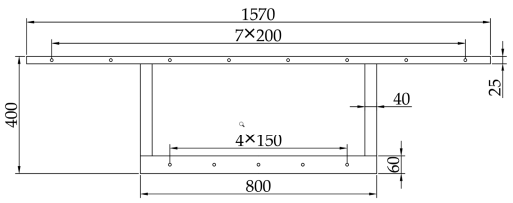

Figure 2. Simplified cross-section of box girder (unit: cm).

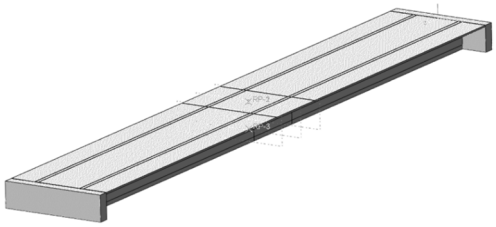

Figure 3. Finite element model of the box girder.

2.2.2. Material Models

In actual bridge operation, the material is mainly in an elastic working state, and the elastic constitutive model is often established in the analysis [12,27]. Based on this fact, this model ignores the influence of material nonlinearity and adopts a linear elastic constitutive model for both concrete and reinforcement. Concrete modulus of elasticity $E = 3.45 \times 10^{10}$ MPa, Poisson's ratio $\mu = 0.2$, $\rho = 2400$ kg/m^3, prestressing tendons modulus of elasticity $E = 2.07 \times 10^{11}$ MPa, Poisson's ratio $\mu = 0.3$, density $\rho = 7800$ kg/m^3.

2.2.3. Loading and Boundary Conditions

This model is a single-span model, in order to simulate the actual working condition of the rigid-frame bridge, the consolidation boundary conditions are adopted at both ends of the box girder for bending moment transfer. In addition, the section of the end is fixed to the surface of the consolidated rigid body in order to prevent stress concentration at the end joints.

Load setting includes dead load and live load, and the gravitational acceleration is set as g = 9.8 m/s^2. The bridge has 4 traffic lanes and the loading form of vehicle loads, according to the Chinese design specification [28], in each lane is shown in Figure 4. The purpose of referring to the specification is to ensure that the bridge produces a live-load response that is as close to the actual situation as possible, so the relevant safety factors are not considered. In order to maximize the mid-span deflection, a concentrated load P_k = 360 kN is applied to the mid-span on all 4 lanes, and a uniform load q_k =10.5 kN/m is distributed over the entire lane.

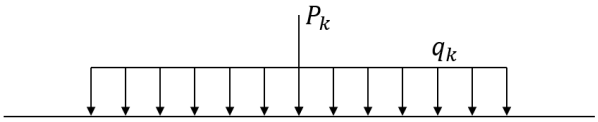

Figure 4. The live-load form applied to each lane.

2.2.4. Element Selection and Mesh

The concrete beam adopts the three-dimensional solid element C3D8R, which is an 8-node hexahedral unit and adopts linear reduction integration. Solid elements can provide the calculation results of three-dimensional stress and more realistically reflect the actual structural response of box girders, with an acceptable computational cost. Along the longitudinal direction, the element length is 50 cm. The mesh discretization of the section is shown in Figure 5. Along the beam height, there are 6 elements of size 54 cm each on the web. The computational efficiency is guaranteed and the analysis accuracy is ensured by this meshing method.

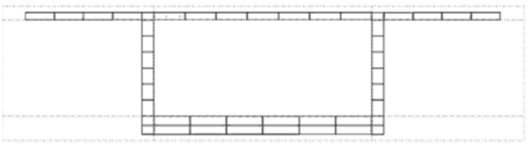

Figure 5. Element mesh in the cross-section.

2.2.5. Comparison Model Settings

In order to compare the influence of casting volume deviation at different positions on the performance, a benchmark model and four comparison models are established. The descriptions are shown in Table 1. The section area of the four comparison models is 10% larger than that of the benchmark model. Since the actual bridge pouring deviation mostly comes from the thickness deviation of each part, and the dimensional deviation of top slab width, bottom slab width, and beam height is relatively small, the principle of increasing the model section area is as follows: only the thickness of each part is changed, and the relative position of the centroid of each part does not change after increasing the area.

Table 1. Detailed description of comparison models and benchmark model.

Model No.	Description	Increase Method	Legend: Red Is the Outline of the Increasing Area
I	Benchmark model	No increase.	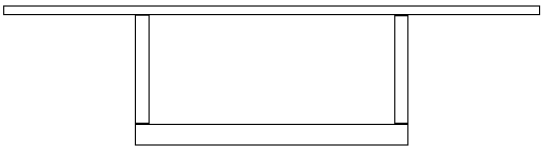
II	10% overall increase	Weighted distribution of each and every part of the top slab, web and bottom slab.	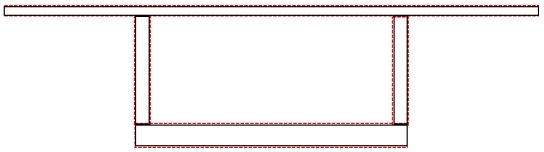
III	10% top slab increase	Increase the same thickness from both sides of the horizontal axis through the centroid of the top slab.	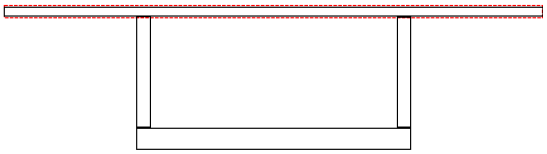
IV	10% web increase	Increase the same thickness from both sides of the vertical axis through the centroid of the web.	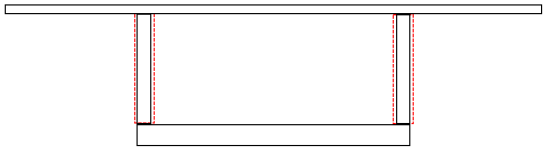
V	10% bottom slab increase	Increase the same thickness from both sides of the horizontal axis through the centroid of the bottom slab.	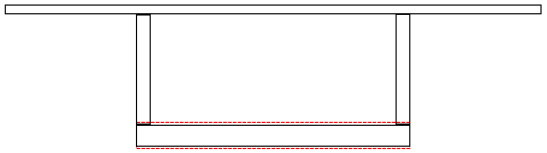

2.2.6. Operating Condition Setting

In order to examine the influence of the casting volume error of the superstructure under different loads, three working conditions are defined: dead load only, live load only, and dead load and live load acting together. The deflection and internal force under live load can simply reflect the stiffness effect caused by the casting volume deviation, the dead-load working condition reflects the macroscopic superposition effect of self-weight constant load change and stiffness change, and the combination of dead-load and live-load working condition demonstrates the performance of the bridge in daily operation.

2.3. Model Calculation Result

The extreme values of deflection and internal force under each working condition are calculated and the results are shown in Table 2. Under the live load-only condition, the deflection of model III with the increase of top slab thickness is the smallest and the most obvious in stiffness improvement, the deflection is reduced by 40.2%. The stiffness of model II increased significantly due to the increase in the weighted area of each part, whose

mid-span deflection is reduced by 18.8%. The increase in web thickness also leads to an increase in stiffness, the deflection γ_{III} decreased by 10.6% compared with γ_I. The increase in bottom-slab thickness has little influence on the stiffness, the deflection decreases by only 1.9%.

Table 2. Mid-span deflections of box girder under different working conditions.

Working Conditions	Deflection γ (mm)					% Ratio of Comparative Model Deflection to Benchmark Model			
	γ_I	γ_{II}	γ_{III}	γ_{IV}	γ_V	$\frac{\gamma_{II}}{\gamma_I}$	$\frac{\gamma_{III}}{\gamma_I}$	$\frac{\gamma_{IV}}{\gamma_I}$	$\frac{\gamma_V}{\gamma_I}$
Dead load	−136.7	−126.7	−108.9	−123.5	−137.6	92.7%	79.7%	90.3%	100.7%
Live load	−40.7	−33.0	−24.3	−36.4	−39.9	81.2%	59.8%	89.4%	98.1%
Combined	−177.3	−159.7	−133.2	−159.8	−177.5	90.1%	75.1%	90.1%	100.1%

Under the dead load-only condition, the deflection of model V is slightly larger than that of the benchmark model, and the deflection of the other models is significantly reduced compared with the benchmark model, indicating that the overall influence of the increase in volume on the models is the increase in the stiffness, among which the increase in the volume of the top slab leads to the most obvious stiffness enhancement. The overall effect of the increase in bottom slab volume is not obvious.

For the casting volume deviation, only considering the change of dead load, the deflection must be increased. In this model, the variation of dead load and stiffness caused by pouring volume deviation are considered at the same time, and the mid-span deflection response is reduced to different degrees. It can be seen that stiffness change caused by pouring volume deviation cannot be ignored. This result is consistent with the general beam theory. For Timoshenko beams, the normal stress of cross section is only related to the calculated position, external force, and cross-section moment of inertia. The further any fiber of the cross-section is from the neutral axis, the greater the contribution of this area to the section moment of inertia [29].

The actual large-span CRCR bridge adopts the form of a variable section, and the height–span ratio and thick–span ratio are related to the position along the span direction, which is different from this model. Based on the actual case, the following paper introduces the distribution characteristics of pouring volume deviation and analyzes the relationship between the pouring deviation of each part of the section and bridge stiffness by establishing a mathematical model.

3. Case Study

3.1. Engineering Background

Bridge A is a four-span continuous rigid-frame bridge with a span arrangement of 59 m + 105 m + 105 m + 59 m. Bridge B is a three-span continuous rigid-frame bridge with a span arrangement of 39 m + 79 m + 39 m, both of which were built in 1996. The section layout and design control dimensions of the two bridges are shown in Figure 6. The cross-section height varies and follows a quadratic curve along the longitudinal bridge direction. As existing indirect measurement methods for operating bridges contains a certain amount of error, with the help of the complete section dimension data obtained after the demolition of the bridge, the indirect measurement error can be avoided, making the measurement data result more accurate and more convincing.

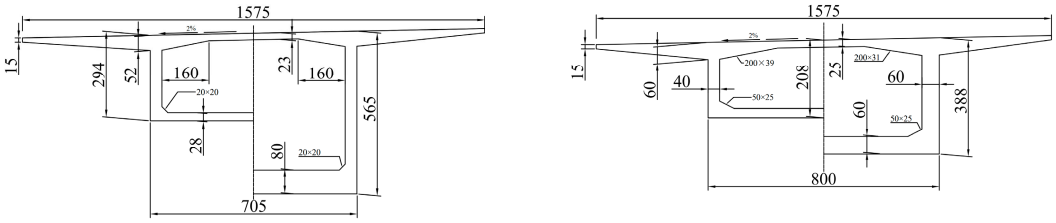

(**a**) (**b**)

Figure 6. Design cross-section layout (unit: cm). (**a**) Bridge A, (**b**) Bridge B.

The demolition of the bridge superstructure adopts the opposite sequence of construction and installation, which is called the "inverted demolition method". Due to severe defects and long-lasting deflection of the two CRCR bridges, for the sake of bridge safety, the superstructure of the two bridges has been dismantled in 2022. After segment 12# of bridge A was released, each beam segment was symmetrically cut and dismantled. A detailed investigation was carried out on the generated cutting surface and the geometric properties of the sections were calculated according to the measured parameters, and compared with the design value to determine the amount of deviation.

There are 136 segments in the double span of bridge A, and 104 segments have been checked. Bridge B has 76 segments, 75 of which have been checked. As shown in Figure 7, shaded sections are completed checks.

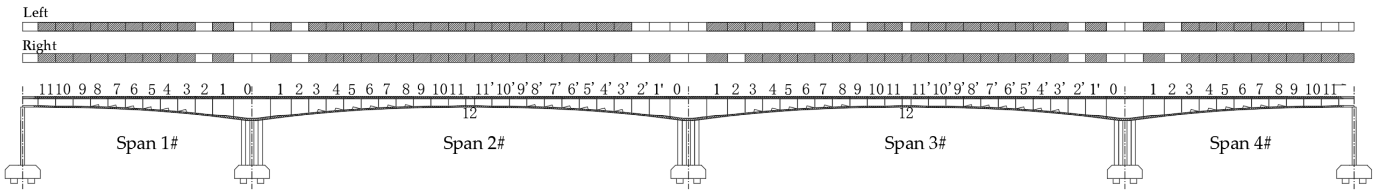

(**a**)

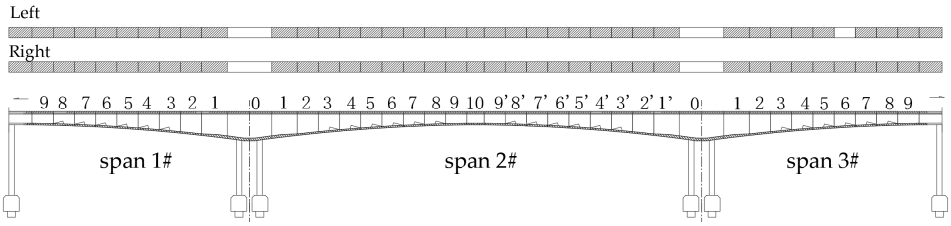

(**b**)

Figure 7. Cross-section inspection status. (The gray block represents the checked section. The number on the beam represents the segment number. The span (·)# is the span number). (**a**) Bridge A, (**b**) Bridge B.

3.2. Measuring Approach

According to the section characteristics of each part, 21 measuring points that reflect the thickness variation characteristics of the box girder are set up. The specific arrangement of measuring points is shown in Table 3 and Figure 8.

Table 3. Notations of sectional dimension and measurement position.

	Web		**Top Slab**
W1	Height of left web	T1	Thickness of left top slab near slabs with haunched ribs
W2	Height of right web	T2	Thickness at the inflection point of left top slab
W3	Thickness of top of left web	T3	Thickness at the inflection point of right top slab
W4	Thickness of bottom of left web	T4	Thickness of right top slab near slabs with haunched ribs
W5	Thickness of top of right web	T5	Width between the inflection point of top slab
W6	Thickness of bottom of right web		
	Flange		**Bottom slab**
F1	Thickness at the edge of left flange	B1	Thickness of left bottom slab near slabs with haunched ribs
F2	Thickness of left flange near slabs with haunched ribs	B2	Thickness of middle of bottom slab
F3	Thickness of right flange near slabs with haunched ribs	B3	Thickness of right bottom slab near slabs with haunched ribs
F4	Thickness at the edge of right flange	B4	Width between the inflection point of bottom slab
F5	width of top slab	B5	Width of bottom slabs outline

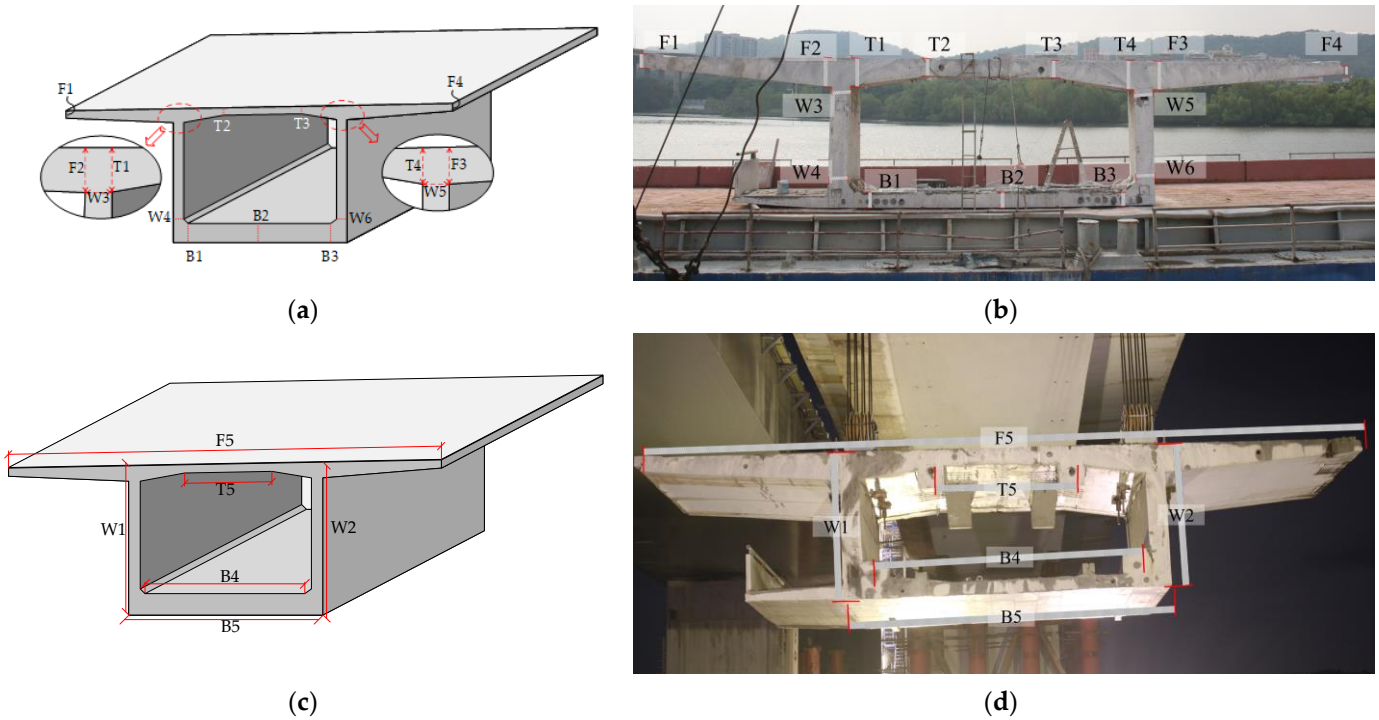

(**a**) (**b**)

(**c**) (**d**)

Figure 8. Cross-sectional measurement position layout. (**a**) Layout of thickness measurement position, (**b**) schematic of thickness measurement position on site, (**c**) layout of outline measurement position, (**d**) schematic of outline measurement position.

The thickness is measured with a T-shaped steel ruler, and the basic contour size of the box girder is measured with a laser rangefinder. The measuring accuracy of the two methods is less than 1 mm, which can meet the requirements of measuring accuracy. The two measuring methods are shown in Figure 9.

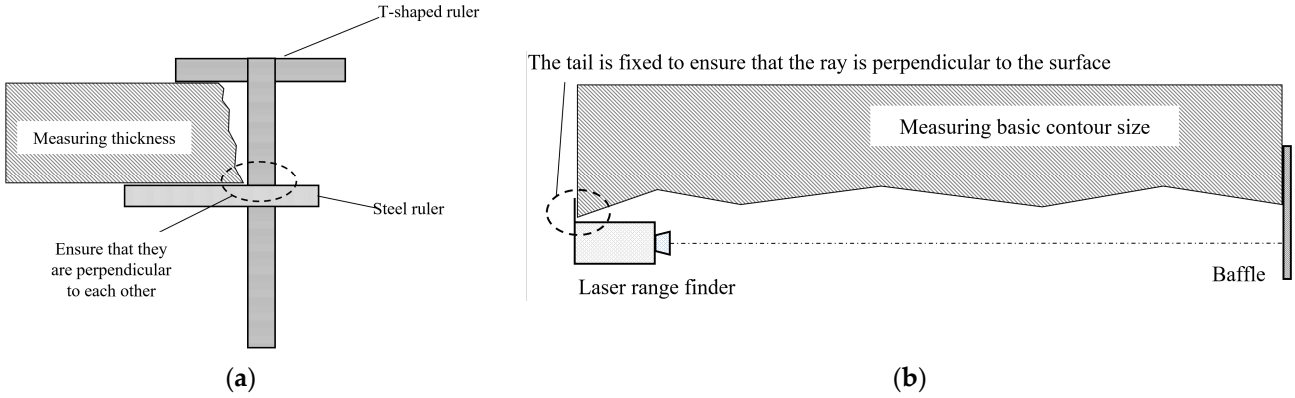

Figure 9. Measurement tools and usage. (**a**) Thickness measurement method, (**b**) Measurement method of outline dimension.

3.3. The Status of PCVD of the Whole Cross Section

Compared to the design, the measured dimension is a random variable. In order to standardize the size of the measured components at variable sections and positions into samples of the same specification, the ratio of the measured section area to the designed section area is adopted as the indicator of deviation rate, namely:

$$K_i = \left(\frac{S_i}{S_k} - 1\right) \times 100\% \quad (1)$$

where K_i is the deviation rate caused by pouring concrete volume deviation; S_i is the section area calculated from the measured data; S_k is the design section area. The K_i of each cross-section of bridge A and bridge B is shown in Figures 10 and 11, respectively.

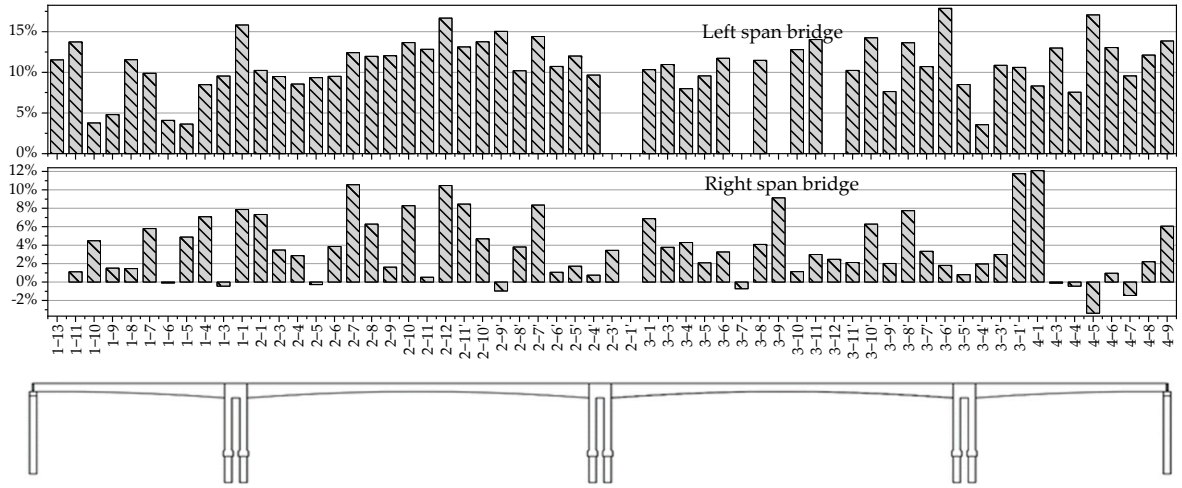

Figure 10. Deviation-rate bar chart of bridge A cross sections.

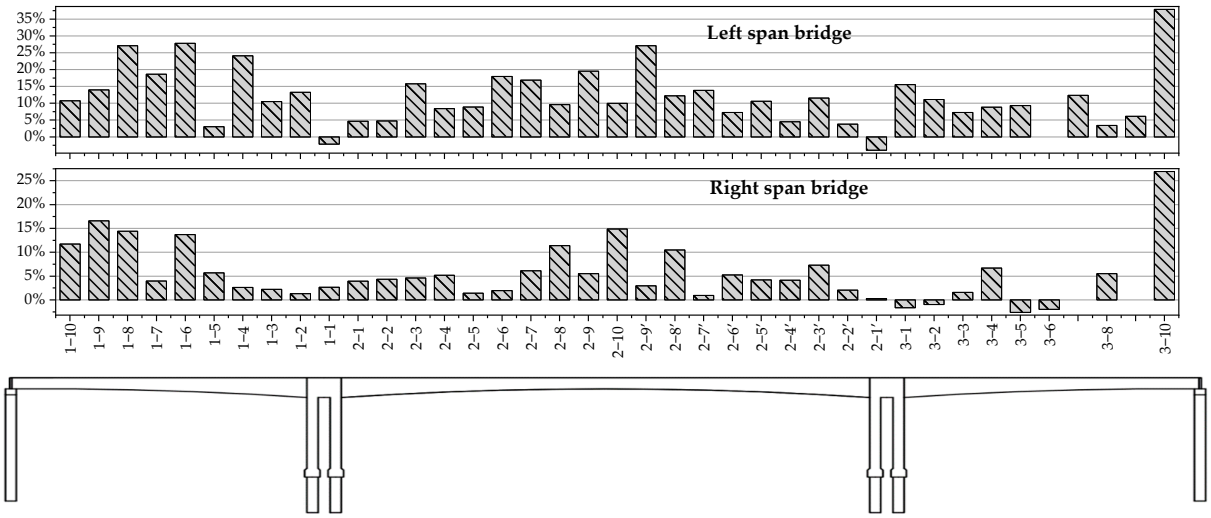

Figure 11. Deviation-rate bar chart of the bridge B cross sections.

As shown in Figure 12, the K_i of each cross-section was statistically analyzed. Moreover, the total number of samples, mean value, standard deviation, and 95% confidence interval were obtained, as shown in Table 4.

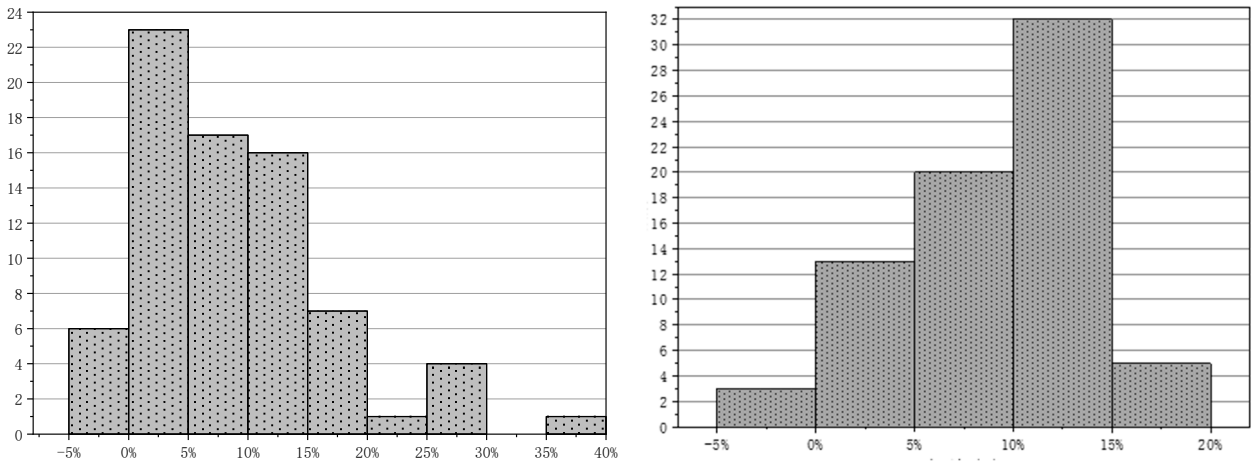

(**a**) (**b**)

Figure 12. Frequency histogram of K_i of each cross-section of bridge A and bridge B, (**a**) bridge A, (**b**) bridge B.

Table 4. Statistical analysis of K_i of bridge A and bridge B.

Bridge	Symbol	Sample Size	Average	Lower 95%	Upper 95%	Standard Deviation	Min	Median	Max
A	K_A	116	7.24%	6.33%	8.16%	4.95%	−3.38%	7.92%	17.87%
B	K_B	75	8.89%	7.04%	10.75%	8.06%	−3.98%	7.27%	37.88%

The measured sectional size is generally larger than the design size, only a few segments are slightly smaller than the design size. The mean deviation rate of bridge A is 7.24%, and ranges from −3.38% to 17.87%. The mean deviation rate of bridge B is 8.89%, and ranges from −3.98% to 37.88%. The 95% confidence intervals of bridge A and B are [6.33%, 8.16%] and [7.04%, 10.75%], respectively.

The deviation rate reaches an extreme value of 37.88% for the section at the end of bridge B, and another extreme value of −3.38% is observed in bridge A. The standard deviations of the two bridges are 4.95% and 8.06%, respectively. It can be seen that the variation in the deviation rate along the bridge is huge.

Assume that the deviation rate K_i follows a normal distribution $N(\mu, \sigma^2)$. Skewness and kurtosis are one of the methods to measure whether a distribution follows a normal distribution [30–33]. According to Demir [34], the kurtosis and skewness of distribution are affected by the sample size, thus the thresholds of skewness and kurtosis should be adjusted accordingly. In this paper, the absolute values of skewness and kurtosis are set to be less than 2.5 and 6, respectively. The skewness and kurtosis are calculated according to Formulas (2) and (3), and the results are shown in Table 5.

$$Skew(K) = E\left[\left(\frac{K-\mu}{\sigma}\right)^3\right] \tag{2}$$

$$Kurt(K) = E\left[\left(\frac{K-\mu}{\sigma}\right)^4\right] \tag{3}$$

where μ and σ is the mean value and standard deviation of K_i, and $E[\cdot]$ is the mathematical expectation.

Table 5. Normal distribution checklist.

Symbol	Skewness	Kurtosis
K_A	−0.02537	−1.04462
K_B	0.16332	1.69674

According to the results of skewness and kurtosis, the deviation rate K_i of bridge A and bridge B conforms to the normal distribution $K_{Ai} \sim N(0.0724, 0.0495^2)$ and $K_{Bi} \sim N(0.0889, 0.0806^2)$, respectively.

3.4. The Status of PCVD of Each Part in Cross-Section

According to the model analysis in Section 2, the impact of pouring deviation on the stiffness of different parts is different. The deviation-distribution characteristics of each part of the two bridges are shown in Figures 13 and 14, and Tables 6 and 7.

Table 6. Statistically analysis of K_i of each part in the cross-section of bridge A.

	Symbol	Average	Standard Deviation	Lower 95%	Upper 95%	Min	Median	Max
Flange	K_{AF}	7.83%	10.35%	5.93%	9.73%	−15.71%	5.64%	32.10%
Top	K_{AT}	7.68%	8.84%	6.05%	9.31%	−15.47%	5.27%	35.89%
Web	K_{AW}	6.38%	7.20%	5.05%	7.70%	−5.82%	5.10%	35.82%
Bottom	K_{AB}	7.70%	7.78%	6.27%	9.13%	−16.06%	7.14%	28.65%

Table 7. Statistically analysis of K_i of each part in the cross-section of bridge B.

	Symbol	Average	Standard Deviation	Lower 95%	Upper 95%	Min	Median	Max
Top	K_{BT}	10.15%	12.26%	7.33%	12.97%	−10.58%	8.67%	56.46%
Web	K_{BW}	5.70%	9.30%	3.55%	7.86%	−17.45%	4.74%	36.28%
Bottom	K_{BB}	10.20%	11.85%	7.48%	12.93%	−9.54%	8.52%	58.27%

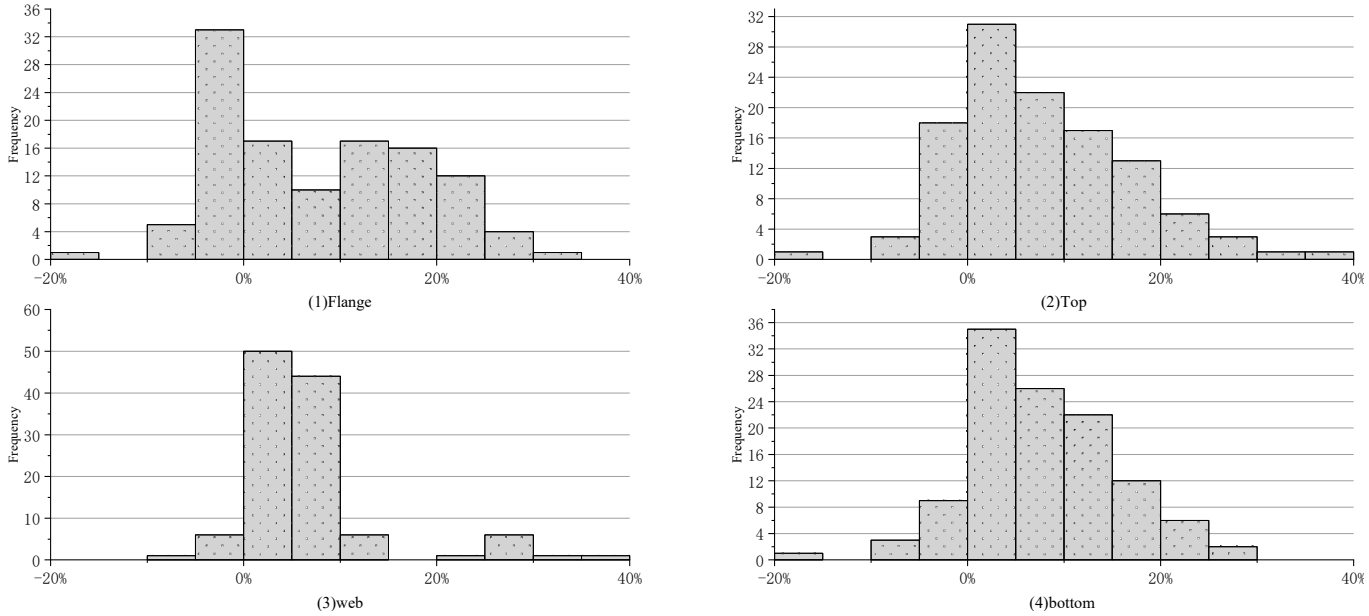

Figure 13. Frequency histogram of K_i of each part in cross-section of bridge A.

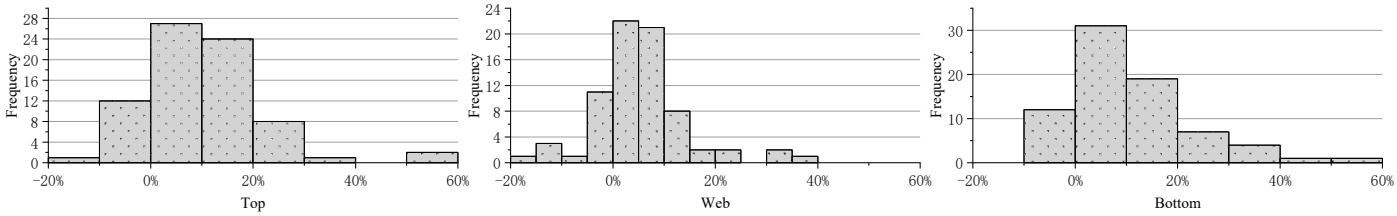

Figure 14. Frequency histogram of K_i of each part in the cross-section of bridge B.

The average deviation rates of the different parts of the cross-section are close to each other. The average deviation rates of the flange, top slab, web plate, and bottom slab of Bridge A are 7.83%, 7.68%, 6.38%, and 7.70%, respectively. The average deviation rates of the top slab, web plate, and bottom slab of Bridge B are 10.15%, 5.70%, and 10.20%, respectively. The deviation rates of different parts of the bridge A cross-section are within the range of −16% to 35%, and the deviation rate of the bridge B cross-section is within the range of −15% to 40%.

The kurtosis and skewness of the deviation rates of the different parts of bridge A and bridge B cross-sections are shown in Table 8. It can be considered that the deviation rates of different parts of a cross-section conform to the normal distribution.

Table 8. Normal distribution checklist.

	Symbol	Skewness	Kurtosis
Bridge A	K_{AF}	0.3826	−0.84707
	K_{AT}	0.70596	0.64497
	K_{AW}	2.24166	5.53851
	K_{AB}	0.2462	0.38215
Bridge B	K_{BT}	1.28908	3.40778
	K_{BW}	0.82647	2.63577
	K_{BB}	1.37295	2.96537

The deviation rate of the same part varies greatly in different positions along the bridge, and occasionally large deviation rate appears. The deviation rate of the bottom

plate of the side span at the end of bridge B reaches 58.27%, and the deviation rate of the web near the pier of bridge B reaches −17.45%

It can be seen that all the high deviation rates of bridge B occur at the end of the side span. A possible reason for this result is that in the bridge design, the section at the end of the bridge span has a different form and dimension than the rest of the sections and needs to be constructed separately. The construction technology at that time is relatively poor and caused problems such as formwork deformation and inaccurate formwork lofting, which in turn led to insufficient fulfillment of the design requirements [35,36]. Additionally, the side span is located on the pier and the deviation has a relatively small impact on the superstructure, making the pouring volume deviation neglected during construction.

3.5. Absolute Quantity Analysis of PCVD of Each Part

The deviation rate characteristics of each part have been described in detail. The deviation rates of each part represent the deviation degree of the actual size relative to the design size. The area of different parts in the box-girder section is different, and the absolute excess square amount varies greatly under the same deviation rate. According to Formula (4), the weighted mean deviation area at different sectional parts is calculated to reflect the contribution degree of deviation at different positions.

$$\sum\left(\bar{K_i} \times \varphi_i\right) \times S_k = S_{Mi} \tag{4}$$

where $\bar{K_i}$ and φ_i are the mean value of deviation rate and weighted area of one part in the cross-section, respectively; $\sum(\cdot)$ is the sum of this particular sectional part over the whole bridge; and S_{Mi} is the weighted mean deviation area of this part.

As can be seen from the calculation results in Figure 15, the influence of both variable and equal-thickness webs on dimensional variation is limited. The weighted deviation area of the bottom slab near the pier are large, indicating that the bottom slab near the pier has a great influence on the deviation of the whole bridge.

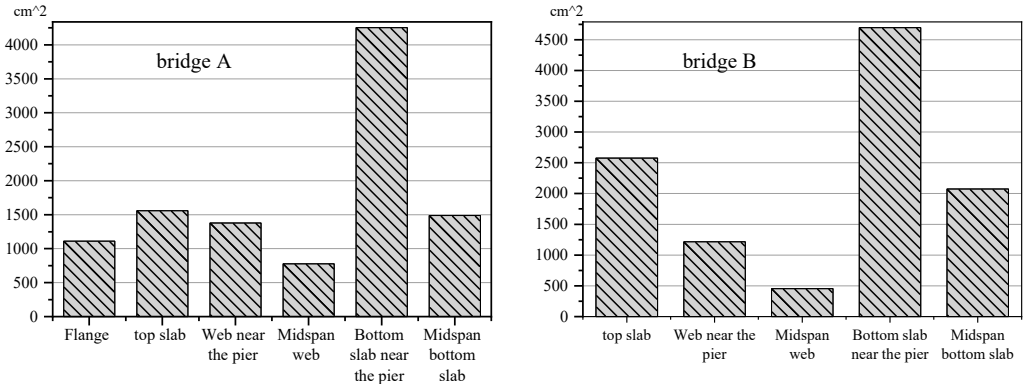

Figure 15. Weighted deviation area at different sectional parts.

3.6. Coefficient of Variation of Dead Load Due to Casting Size Deviation

The cross-section casting deviation rate follows a normal distribution. When considering the dead-load variation caused by the casting size deviation, the design and operation period calculation of continuous rigid-frame bridges should adopt the probability limit state design method to ensure that the load value takes into account the influence of casting deviation within a certain probability. The load value should be calculated according to Formula (5):

$$W_k = W_0 + W_0(\mu_W + \alpha_W \sigma_W) \tag{5}$$

where W_k is the value of dead load considering the PCVD, W_0 is the standard value of dead load, μ_W is the average deviation rate of the whole cross-section, α_W is reliability coefficient

corresponding to the specified probability of W_k, and σ_W is the standard deviation of the deviation rate of the whole cross-section.

Let c_W be the coefficient of dead load due to casting deviation, and the calculation formula of c_W is as follows.

$$c_W = 1 + \mu_W + \alpha_W \sigma_W \tag{6}$$

When the specified probability W_k is set to 95%, the corresponding reliability coefficient α_W = 1.645, and the c_W of bridge A and bridge B are 1.15 and 1.22, respectively. It is necessary to consider c_W when considering the variation of dead load caused by casting deviation.

4. Analysis of the Influence of PCVD on Stiffness

The deflection of the beam with variable section is closely related to the external force and the section moment of inertia. The calculation formulas of deflection in literature [12,13] all show that the deflection is related to the section moment of inertia. The cross-section moment of inertia is selected as the index to reflect the macroscopic stiffness of the bridge, and the stiffness deviation coefficient c is defined to reflect the influence of pouring volume deviation on the bridge stiffness. The stiffness deviation coefficient c calculated as shown in Formula (7).

$$\frac{\mathrm{I}}{\mathrm{I}'} - 1 = c \tag{7}$$

where I and I′ are section moment of inertia calculated by measured value and designed value, respectively.

The frequency distribution histogram of c of bridge A is shown in Figure 16, and the descriptive statistics are shown in Table 9.

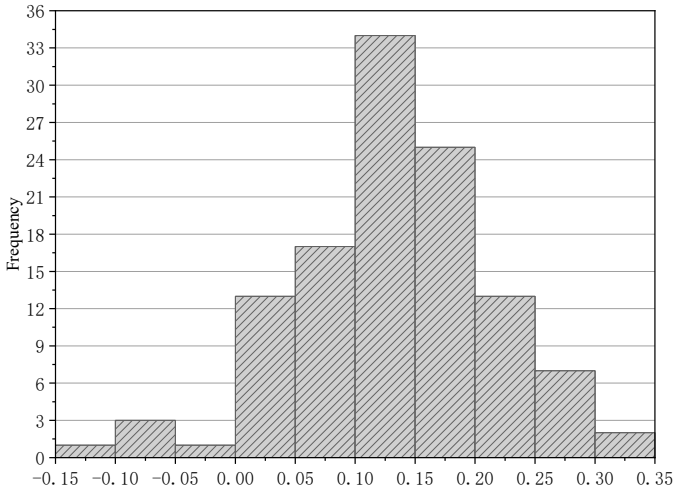

Figure 16. Frequency histogram of c of bridge A.

Table 9. Statistically analysis of c of bridge A.

Sample Size	Average	Standard Deviation	Skewness	Kurtosis	Median	Lower 95%	Upper 95%
116	0.1338	0.0819	−0.2876	0.5849	0.1367	0.1187	0.1488

From the value of eccentricity kurtosis, it can be estimated that the stiffness correction coefficient $c \sim N(0.13377, 0.08187^2)$, the mean stiffness correction coefficient is 0.013377 and ranges from −0.138 to 0.327, and the 95% confidence interval is [0.11871, 0.14882].

As mentioned above, the variation of the moment of inertia of the section is affected differently by the deviation of each part. With the deviation rate of each part of each section as the independent variable and the deviation coefficient of stiffness of each section as

the dependent variable, a multiple linear regression model was established, as shown in Formula (8), and the least-square method was used for fitting.

$$c = \beta_1 K_{AF} + \beta_2 K_{AT} + \beta_3 K_{AW} + \beta_4 K_{AB} + \mathrm{C} \quad (8)$$

where β_1, β_2, β_3 and β_4 are regression coefficients, C is the intercept.

There are 116 observed values, and the fitting results are as follows: β_1 = 0.130121, β_2 = −0.00244, β_3 = 0.110192, β_4 = 0.75923, C = 0.058293.

Multiple R = 0.748, indicating that the casting size deviation of each part has a strong correlation with the change of section moment of inertia. F-test was used to determine whether the global linear relationship of the independent variable was significant. F = 35.3, significance F = $5.2 \times 10^{-19} < 0.01$, in general, the pouring deviation ratio of all parts had a strong correlation with the stiffness-deviation coefficient, indicating a strong significance.

An Independent sample *t*-test was conducted for each parameter. The hypothesis was set as β_i = 0, i = 1, 2, 3, 4. The t statistic and the hypothesis probability *p*-value of each parameter are shown in Table 10. At the 95% confidence level, β_2 and β_3 both have poor significance and cannot meet the standard, so it can be concluded that the hypothesis is true, that is, β_2 and β_3 = 0.

Table 10. Statistical analysis of parameters.

	Coefficients	**Standard Error**	**T Stat**	***p*-Value**
C	0.058	0.010	5.882	4.36×10^{-8}
β_1	0.130	0.059	2.192	0.030
β_2	−0.002	0.070	−0.035	0.972
β_3	0.110	0.073	1.517	0.132
β_4	0.759	0.068	11.163	7.44×10^{-20}

The fitting formula is shown in (9). It can be seen from the parameter values that the casting size deviation of the flange and the bottom slab has a significant impact on the stiffness deviation coefficient. Due to the change of the actual CRCR bridge section along the bridge direction, it can be seen from the analysis of the absolute value of the casting size deviation in Section 3.5 that the deviation of the bottom slab dominates near the pier position, so it is reasonable that the bottom plate has a significant impact on the stiffness deviation coefficient.

$$c = 0.13 K_{AF} + 0.75 K_{AB} + 0.06 \quad (9)$$

Based on the survey results mentioned above, for the inspection of an existing continuous rigid-frame bridge, the mean value can be considered, that is, c_S = 0.13; for the design of cantilever cast continuous rigid-frame bridge, the lower limit value in the 95% confidence interval of the statistical quantity can be considered, that is, c_S = 0.12.

5. Conclusions

In this paper, the finite element method, actual case investigation and statistical analysis were used to analyze the structure performance impact on the variation of dead load and cross-section stiffness caused by PCVD of CRCR bridges. The main conclusions are as follows:

1. The influence of volume deviation at different positions within the cross-section on the cross-sectional stiffness varies. The structural stiffness is more sensitive to the thickness of the top slab and the flange. The combined effect of dead-load variation and cross-sectional stiffness variation on structural performance is uncertain and may be beneficial or detrimental to structural performance. Specific analysis of the actual research object is required.
2. The section deviation rate is in the range of 6.33~10.75% at the 95% confidence interval, and the deviation rate of different sectional parts is in the range of 5.05~12.97%, which

indicates that the cast-in-place concrete bridge with cantilever generally has PCVD. The maximum standard deviation is 12.26%, which indicates that the amount of deviation is random and scattered.

3. The weighted mean deviation value of each part was calculated, and the results showed that the near pier bottom slab, mid-span bottom slab and top slab have larger deviation values, which may have a more pronounced effect on the dead load. Among them, the near pier bottom slab is most likely to a produce larger deviation value and should be the part of primary concern when studying dead-load variation.
4. In this paper, the dead-load deviation coefficient c_W and the stiffness deviation coefficient c have been proposed for the assessment procedure of the influence of PCVD on existing bridges' performance. This case study can serve as a benchmark for guiding the internal-force calculation and service state analysis of bridges of the same type.

Author Contributions: Conceptualization, J.Z. and P.L.; methodology, P.L.; software, J.Y.; validation, X.H., J.Z. and P.L.; formal analysis, J.Y.; investigation, J.Y.; resources, J.Z. and P.L.; data curation, J.Y.; writing—original draft preparation, J.Y.; writing—review and editing, X.H., J.Z. and P.L.; visualization, J.Y. and X.H.; supervision, X.H., J.Z. and P.L.; project administration, P.L.; funding acquisition, J.Z. All authors have read and agreed to the published version of the manuscript.

Funding: This research was funded by Research Institute of Highway Ministry of Transport and the project named "Key Technology Research of Guanfo Expressway Maintenance Engineering".

Data Availability Statement: Data from this study can be made available upon request.

Conflicts of Interest: The authors declare no conflict of interest.

References

1. Wang, H.L.; Xie, C.L.; Liu, D.; Qin, S.F. Continuous Reinforced Concrete Rigid-Frame Bridges in China. *Pract. Period. Struct. Des. Constr.* **2019**, *24*, 05019002. [CrossRef]
2. Zhai, Z.P.; Li, Y.Z.; Guo, W. The Shear-lag Effect of Thin-walled Box Girder under Vertical Earthquake Excitation. In Proceedings of the International Conference on Advances in Materials, Machinery, Electronics (AMME), Wuhan, China, 25–26 February 2017.
3. Sa-Nguanmanasak, J.; Chaisomphob, T.; Yamaguchi, E. Stress concentration due to shear lag in continuous box girders. *Eng. Struct.* **2007**, *29*, 1414–1421. [CrossRef]
4. Tan, M.Y.; Cheng, W.M. Nonlinear Buckling Analysis of Thin-Walled Box Beams considering Shear Lag. *Math. Probl. Eng.* **2020**, *2020*, 05019002. [CrossRef]
5. Zhou, M.D.; Zhang, Y.H.; Lin, P.Z.; Zhang, Z.B. A new practical method for the flexural analysis of thin-walled symmetric cross-section box girders considering shear effect. *Thin-Walled Struct.* **2022**, *171*, 108710. [CrossRef]
6. Liu, J.; Huang, X.Y.; Chen, J.J.; Wu, Q.Y. Effect of Shear Deformation at Segmental Joints on the Short-Term Deflection of Large-Span Cantilever Cast Prestressed Concrete Box Girders. *Buildings* **2023**, *13*, 219. [CrossRef]
7. Barr, P.J.; Stanton, J.F.; Eberhard, M.O. Effects of Temperature Variations on Precast, Prestressed Concrete Bridge Girders. *J. Bridge Eng.* **2005**, *10*, 186–194. [CrossRef]
8. Dilger, W.H.; Ghali, A.; Chan, M.; Cheung, M.S.; Maes, M.A. Temperature stresses in composite box girder bridges. *J. Struct. Eng. ASCE* **1983**, *109*, 1460–1478. [CrossRef]
9. Yu, Q.; Bazant, Z.P.; Wendner, R. Improved Algorithm for Efficient and Realistic Creep Analysis of Large Creep-Sensitive Concrete Structures. *ACI Struct. J.* **2012**, *109*, 665–675.
10. Bazant, Z.P.; Yu, Q.; Li, G.H. Excessive Long-Time Deflections of Prestressed Box Girders. I: Record-Span Bridge in Palau and Other Paradigms. *J. Struct. Eng. ASCE* **2012**, *138*, 676–686. [CrossRef]
11. Guo, F.; Yang, Y.Q.; Huang, S.Q. Research on Deflection and Cracking of Prestressed Concrete Continuous Girder Bridge. In Proceedings of the 2nd Global Conference on Civil, Structural and Environmental Engineering (GCCSEE 2013), Shenzhen, China, 28–29 September 2013; pp. 1014–1017.
12. Lin, L.X.; Zhang, Y.H.; Wu, Y.P.; Ding, N.H. Approximate Deflection Calculation of Variable Box Section Girder Considering the Effect of Shear Lag and Shear Deformation. In Proceedings of the International Conference on Civil Engineering and Building Materials (CEBM), Kunming, China, 29–31 July 2011; pp. 967–971.
13. Ostwald, M.; Magnucki, K.; Rodak, M. Bicriteria optimal design of open cross sections of cold-formed thin-walled beams. *Steel Compos. Struct. Int. J.* **2007**, *7*, 53–80. [CrossRef]
14. Bazant, Z.P. RILEM Technical Committee TC-242-MDC. RILEM draft recommendation: TC-242-MDC multi-decade creep and shrinkage of concrete: Material model and structural analysis Model B4 for creep, drying shrinkage and autogenous shrinkage of normal and high-strength concretes with multi-decade applicability. *Mater. Struct.* **2015**, *48*, 753–770. [CrossRef]

15. Jaishi, B.; Ren, W.X. Finite element model updating based on eigenvalue and strain energy residuals using multiobjective optimisation technique. *Mech. Syst. Signal Process.* **2007**, *21*, 2295–2317. [CrossRef]
16. Pereira, M.; Glisic, B. A hybrid approach for prediction of long-term behavior of concrete structures. *J. Civ. Struct. Health Monit.* **2022**, *12*, 891–911. [CrossRef]
17. Ren, W.X.; Chen, H.B. Finite element model updating in structural dynamics by using the response surface method. *Eng. Struct.* **2010**, *32*, 2455–2465. [CrossRef]
18. Wu, J.; Cheng, F.; Zou, C.; Zhang, R.T.; Li, C.; Huang, S.P.; Zhou, Y. Swarm Intelligent Optimization Conjunction with Kriging Model for Bridge Structure Finite Element Model Updating. *Buildings* **2022**, *12*, 504. [CrossRef]
19. Zhou, L.R.; Wang, L.; Chen, L.; Ou, J.P. Structural finite element model updating by using response surfaces and radial basis functions. *Adv. Struct. Eng.* **2016**, *19*, 1446–1462. [CrossRef]
20. Mutashar, R.; Sargand, S.; Khoury, I.; Al Rikabi, F.T. Influence of Nonuniform Box Beam Dimensions and Bridge Transverse Slope on Environmentally Induced Stresses in Adjacent Box Beam Bridges. *J. Perform. Constr. Facil.* **2018**, *32*, 1063–1067. [CrossRef]
21. Holicky, M.; Markova, J. Effect of geometric deviations on reliability of a reinforced concrete slab. In Proceedings of the Symposium on Advanced Design of Concrete Structures, Gothenburg, Sweden, 12–14 June 1997; pp. 319–326.
22. Luo, X.Y.; Long, H.; Dong, S.; Wu, J.Y. Prefabricated Concrete Component Geometry Deviation Statistical Analysis. *Math. Probl. Eng.* **2021**, *2021*, 9993451. [CrossRef]
23. Lee, H.M.; Kwon, Y.H.; Park, H.S.; Lee, I. Displacement measurement of an existing long span steel box-girder using terrestrial laser scanning. In Proceedings of the 7th International Conference on Damage Assessment of Structures (DAMAS 2007), Turin, Italy, 25–27 June 2007; p. 511.
24. Truong-Hong, L.; Lindenbergh, R. Automatically extracting surfaces of reinforced concrete bridges from terrestrial laser scanning point clouds. *Autom. Constr.* **2022**, *135*, 104127. [CrossRef]
25. AASHTO. *AASHTO LRFD Bridge Design Specifications*, 3rd ed.; AASHTO LRFD: Washington, DC, USA, 2017.
26. *JTG D60-2015*; General Specification for Design of Highway Bridge and Culverts. People's Communications Publishing Co., Ltd.: Beijing, China, 2015.
27. Zhang, N.H.; Xing, J.J. An alternative model for elastic bending deformation of multilayered beams. *J. Appl. Phys.* **2006**, *100*, 103519. [CrossRef]
28. *JTG 3362-2018*; Specifications for Design of Highway Reinforced Concrete and Prestressed Concrete Bridges and Culverts. People's Communications Publishing Co., Ltd.: Beijing, China, 2018.
29. Gere, J.M.; Timoshenko, S.P. *Mechanics of Materials*; Stanley Thornes: Cheltenham, UK, 1999.
30. Bai, J.S.; Ng, S. Tests for skewness, kurtosis, and normality for time series data. *J. Bus. Econ. Stat.* **2005**, *23*, 49–60. [CrossRef]
31. Blanca, M.J.; Arnau, J.; Lopez-Montiel, D.; Bono, R.; Bendayan, R. Skewness and Kurtosis in Real Data Samples. *Methodol. Eur. J. Res. Methods Behav. Soc. Sci.* **2013**, *9*, 78–84. [CrossRef]
32. Boutahar, M. Behaviour of skewness, kurtosis and normality tests in long memory data. *Stat. Methods Appl.* **2010**, *19*, 193–215. [CrossRef]
33. Nguyen, T.Q.; Tran, L.Q.; Nguyen-Xuan, H.; Ngo, N.K. A statistical approach for evaluating crack defects in structures under dynamic responses. *Nondestruct. Test. Eval.* **2021**, *36*, 113–144. [CrossRef]
34. Demir, S. Comparison of Normality Tests in Terms of Sample Sizes under Different Skewness and Kurtosis Coefficients. *Int. J. Assess. Tools Educ.* **2022**, *9*, 397–409. [CrossRef]
35. Talesnick, M.; Katz, A. Measuring lateral pressure of concrete: From casting through hardening. *Constr. Build. Mater.* **2012**, *34*, 211–217. [CrossRef]
36. Kwon, S.H.; Shah, S.P.; Quoc, T.P.; Kim, J.H.; Lee, Y. Intrinsic Model to Predict Formwork Pressure. *ACI Mater. J.* **2010**, *107*, 20–26.